Iranian Journal of Materials Science and Engineering, Vol. 21, Number 4, December 2024
RESEARCH PAPER

The Potential of Silver-Doped Zinc Sulfide/Cadmium Sulfide Nanocomposites in Optoelectronic Applications

Maryam Hajiebrahimi[1], Sanaz Alamdari[2,*], Omid Mirzaee[1,*]

** o_mirzaee@semnan.ac.ir, s.alamdari@semnan.ac.ir*

[1] Faculty of Materials and Metallurgical Engineering, Semnan University, Semnan, Iran
[2] Department of Nanotechnology, Faculty of New Sciences and Technologies, Semnan University, Semnan, Iran

Received: October 2024 **Revised: December 2024** **Accepted: December 2024**
DOI: 10.22068/ijmse.3784

Abstract: *Dual nanocomposites based on metal sulfide nanomaterials with a narrow band gap are favorable candidates for future optoelectronic applications and ionizing ray sensors. This study synthesised novel silver-doped zinc sulfide/ cadmium sulfide (ZnS/CdS: Ag) nanocomposites using the cost-effective solvothermal approach. For the first time, the radiation sensitivity of the newly developed nanocomposite was assessed using a 241 Am alpha source and ion beam-induced luminescence (IBIL) measurements. When measured at room temperature, the ZnS/CdS: Ag nanocomposite demonstrated significant light emission in the blue-green spectrum. When exposed to alpha irradiation, the ZnS/CdS: Ag nanocomposite film displayed exceptional sensitivity compared to pure ZnS or CdS films. The FESEM images revealed a uniform distribution of semi-spherical and rod-shaped nanoparticles, with an average particle size of 180 nm for both shapes. The results from XRD and EDX demonstrated distinct peaks corresponding to ZnS, CdS, and associated elements within the nanocomposite. The existence of several functional groups within the nanocomposite was confirmed through Fourier transform infrared spectroscopy. Evaluations revealed that the optical quality of the ZnS/CdS: Ag nanocomposite showed enhancement compared to pure ZnS and CdS. The results suggest that the ZnS/CdS: Ag nanocomposite film holds great promise for applications in optoelectronic devices and detection technologies.*

Keywords: *Ag dopant, Dual nanocomposite, Luminescence, Optical properties, Scintillation response.*

1. INTRODUCTION

Scintillators, materials capable of converting high-energy rays or particles into low-energy visible photons, play a crucial role in radiation detection. These materials are widely used in space exploration, non-intrusive security checks, and medical imaging, with significant advancements in recent years [1-6]. However, most commercial scintillators are in fragile crystal forms and require complex, time-consuming, and expensive preparation [3]. This limitation underscores the need for innovative approaches to produce highly luminescent materials in more practical forms. One promising alternative is the development of flexible scintillator nanocomposites made from luminescent nanopowders incorporated into polymeric matrices [7]. These nanocomposites, particularly those based on semiconductor materials, can potentially improve the performance of optoelectronic devices, including scintillators, by offering enhanced optical properties and better charge separation. Nanostructures and nanocomposites based on semiconductors have a wide range of tunable optical characteristics, highly desirable in fields like photonics, energy conversion, sensing, and advanced optical materials [9-11]. Combining semiconductors with compatible band energy levels enhances optical properties through more effective carrier separation and interfacial charge transfer efficiency [12]. These hybrid semiconductor systems often exhibit intriguing optical properties, leading to rapid advancements in the study of scintillation mechanisms and applications [4, 5, 13]. Among semiconductor nanomaterials, metal sulfides, such as zinc sulfide (ZnS) and cadmium sulfide (CdS), are particularly interesting due to their unique electrical and optical characteristics. ZnS is a wide bandgap semiconductor with excellent optical properties, including high transparency in visible and UV regions, strong luminescence, and large exciton binding energy [14-17]. CdS, in contrast, is known for its exceptional scintillation performance, high stopping power, efficiency, and chemical stability, making it ideal for various technical applications [18, 19]. When these two materials are combined, they form nanocomposites that enhance optical properties, such as luminescence and charge transfer, due to their complementary bandgap characteristics [5, 17, 21]. Furthermore, doping these materials with elements like silver can significantly modify their

[DOI: 10.22068/ijmse.3784]

optical and electronic properties, improving their efficiency for optoelectronic applications.

Recent advancements in optoelectronic devices have focused on developing novel materials and enhanced optical properties to improve device performance. Key progress areas include luminescent materials, semiconductors with tailored bandgaps, and the integration of hybrid and doped systems for improved functionality [22]. Doping is a widely used technique in semiconductor material engineering, allowing for control over the material's electronic structure and enhancing its performance in various devices. By introducing silver nanoparticles as a dopant, ZnS/CdS nanocomposites can benefit from silver's unique electronic, catalytic, and optical properties, further improving their scintillation and optoelectronic properties [23, 24]. This approach facilitates the design of materials with optimized band energy levels, leading to improved charge separation, enhanced luminescence, and better overall performance in radiation detection and optoelectronic devices.

Consequently, enhancing the optical properties of materials can be achieved through doping or the combination of dual oxide and sulfide semiconductors, creating novel nanocomposites with appropriate band energy levels and distinct characteristics. A recent study highlights the strong UV photoluminescence emission of ZrO_2 nanostructures, which indicates their high purity and excellent crystallinity. These properties position ZrO_2 nanostructures as promising candidates for UV-based optoelectronic applications, demonstrating their potential in devices that rely on efficient UV light emission [25]. Another study successfully synthesized ZnO/CWO: Ce nanocomposites using a straightforward process, followed by an investigation into the optical response of the samples under ionizing radiation and UV light [4]. The findings revealed a notably enhanced optical response in the ZnO/CWO: Ce nanocomposite compared to ZnO/CWO and the individual ZnO and CWO samples [5]. Additionally, it has been reported that a chitosan-based on a $BaWO_4$ sensor that was fabricated exhibited a high degree of sensitivity and flexibility in response to laser, UV, proton, and alpha irradiation that can be a good candidate in optoelectronic applications [26]. Furthermore, it is possible to introduce a variety of inorganic or organic components to modify the optoelectronic properties of these mixed oxide materials. For instance, the flexible nanocomposite can boost its photosensitivity through Förster resonance energy transfer (FRET) between the polymer matrix and the nanostructured additives [27]. Another recent study found that flexible mixed oxide thin films, specifically ZnO(Ag)/PWO(Er) embedded in a polyvinyl alcohol matrix, exhibited high sensitivity to ionizing radiation [28]. Moreover, a study on optoelectronic applications highlights the luminescence properties of cerium-doped zinc oxide/cadmium tungstate ($ZnO/CdWO_4$: Ce) nanocomposite particles. The findings indicate that these nanocomposites demonstrate enhanced luminescence and excellent thermal stability, positioning them as promising candidates for advanced optoelectronic devices [29].

In this study, the synthesis of ZnS/CdS: Ag flexible films utilizing a PVA matrix through a solvothermal chemical method. The potential for photonic applications was explored by examining the structural and optical properties of the materials under UV light, ion beam exposure, and alpha irradiation at room temperature. This work introduces an innovative approach by creating flexible thin films composed of mixed sulfides within a PVA matrix, emphasizing customized band energy levels, cost-effective techniques, and the possibilities for enhancing smart textiles and sensor technologies.

2. EXPERIMENTAL PROCEDURES

2.1. Material and Chemicals

In this study, all materials and chemical reagents were used as obtained, with no further purification. The key reagents included zinc acetate dihydrate [$Zn(CH_3CO_2)_2 \cdot 2H_2O$, Merck, 99.9% purity], cadmium acetate dihydrate [$Cd(CH_3COO)_2 \cdot 2H_2O$, Sigma-Aldrich, 99.9% purity], sodium sulfide [$Na_2S \cdot 9H_2O$, Sigma-Aldrich, 99.9% purity], silver nitrate [$AgNO_3$], and ethanol (99.9% purity). Deionized water was used consistently throughout all experimental procedures.

2.2. Synthesize of ZnS and CdS Nanoparticles

In a typical procedure to synthesize zinc sulfide (ZnS) nanoparticles, zinc acetate and sodium sulfide were first dissolved in 50 ml of deionized

[DOI: 10.22068/ijmse.3784]

water. Using a co-precipitation method, the sodium sulfide solution was carefully added drop by drop into the zinc acetate solution. The resulting mixture was then centrifuged three times to remove any impurities and dried at 80°C for 24 hours. The dried sample was heated to 800°C in a furnace for one hour to complete the synthesis, yielding ZnS powder. A similar co-precipitation technique was used for cadmium sulfide (CdS) nanoparticles. Cadmium acetate dihydrate and sodium sulfide were dissolved separately in deionized water at an equal molar ratio. Next, the sodium sulfide solution was slowly introduced into the cadmium acetate solution, prompting the formation of a precipitate. This precipitate was thoroughly washed, centrifuged, and dried at 80°C for 24 hours. Finally, the sample was calcined at 600°C for two hours, forming CdS nanoparticles.

2.3. Synthesize of ZnS/CdS: Ag Dual Nanocomposite

Solvothermal synthesis and sonication were used to produce Ag-doped ZnS/CdS nanocomposite. 20 ml of ethanol was mixed with ZnS and CdS at a molar ratio of 1:1. The resultant solution was dissolved with a magnetic stir and then in an ultrasonic bath for 15 min. Finally, the obtained mixture was transferred in a PTFE-lined autoclave and heated to 110°C. After 12 h, the resultant solution was centrifuged, washed, and dried in the oven.

2.4. Preparation of ZnS/CdS: Ag@PVA Flexible Nanocomposite Film

To analyze the alpha radiation response of our samples, we began by dissolving 2 gr of polyvinyl alcohol (PVA, Sigma-Aldrich) in 20 ml of deionized (DI) water, stirring it for three hours to ensure complete dissolution. Separately, 0.5 gr of ZnS/CdS: Ag powder was mixed with 5 ml of DI water and then gradually added to the PVA solution, continuously stirring for another three hours to achieve a uniform mixture. The resulting paste-like composite was evenly spread onto a glass plate and left to air-dry at room temperature. After 24 hours, the polymer composite sheets could be easily peeled off and trimmed into square film samples, yielding flexible nanocomposite films. Figure 1 provides a visual guide to the ZnS/CdS: Ag nanocomposite preparation process.

2.5. Characterization

The crystalline structure and phase of the material were characterized using X-ray diffraction (XRD) on a Bruker D8-Advance system. Field emission scanning electron microscopy (FESEM, TESCAN) was applied to assess the materials' morphology and elemental composition.

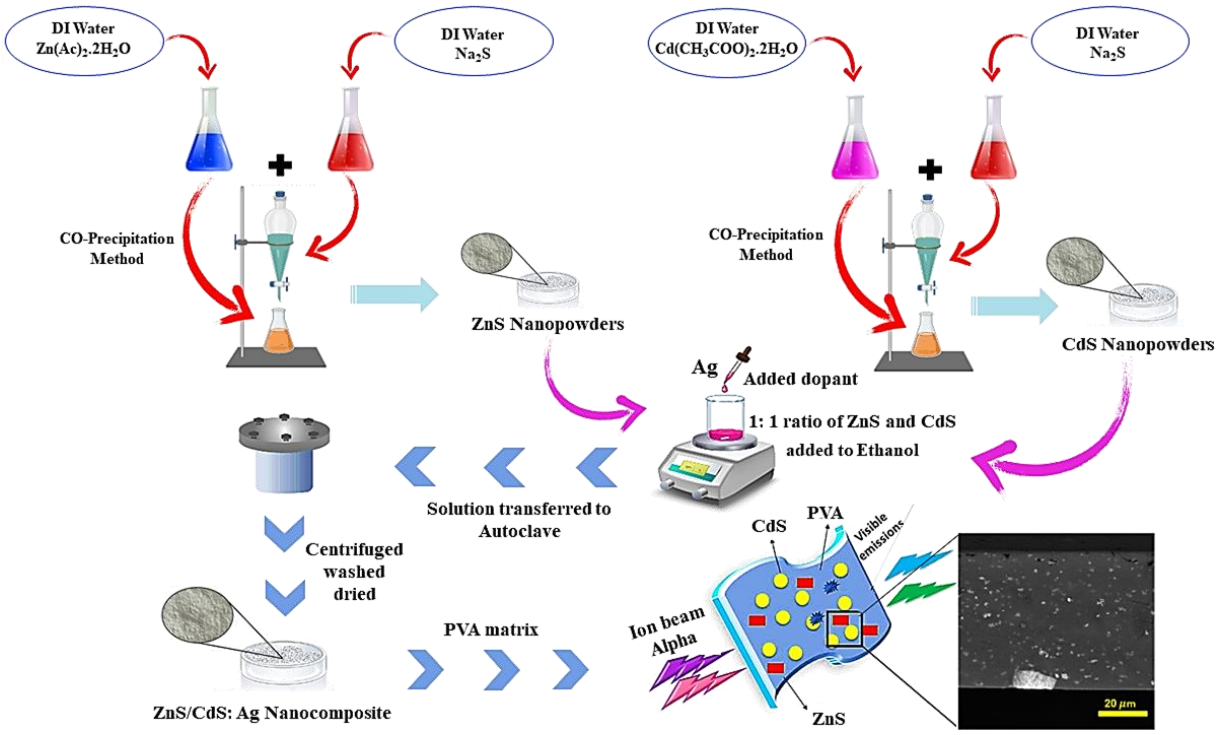

Fig. 1. Experimental process

[DOI: 10.22068/ijmse.3784]

Functional groups and vibrational modes were analyzed via Fourier-transform infrared (FTIR) spectroscopy with a PerkinElmer instrument.
UV-visible diffuse reflectance spectra were recorded using a Perkin-Elmer LS-5 for optical properties. Ion beam-induced luminescence (IBIL) measurements were conducted at room temperature with a 2.25 MeV proton beam at 4 nA current. To evaluate the radiation response, flexible composite films were affixed to a photomultiplier (Model FEU_31, Russia) using optical grease, and count rates were recorded with a 241 Am alpha source (activity 0.09 μci) and collimated rays. A preamplifier, an amplifier, a high voltage power supply, and a data acquisition system were all parts of the electronic devices used (MCA-P3100DP-Parto Negar Shahab Company-Radonik).

3. RESULTS AND DISCUSSION

3.1. XRD

An X-ray diffraction analysis was performed to examine the crystalline structure of pure ZnS, CdS, and the ZnS/CdS: Ag nanocomposite. Figure 2 illustrates the XRD patterns for all the samples analyzed. The angles 2θ= 26.94°, 28.56°, and 31.55°, which are the most intense diffraction peaks, correspond to the lattice planes (100), (002), and (101). The lattice constants reveal a hexagonal structure, with values of a= 0.3821 nm and c= 0.6257 nm [30]. The standard data for the hexagonal structure of ZnS (JCPDS card no. 00-036-1450) was well-matched by the ZnS peaks. In addition, the diffraction peaks of pure CdS can be exclusively indexed as the hexagonal of CdS, which is in excellent agreement with the reported data (JCPDS card no. 01-077-2306). The XRD pattern of the ZnS/CdS: Ag nanocomposite indicates the simultaneous presence of hexagonal ZnS and hexagonal CdS structures. In comparison to pure ZnS and CdS, the nanocomposite sample exhibited a slight shift in the diffraction peaks, indicating the possible incorporation of Zn ions into the CdS lattice as a crystalline defect or the formation of a new compound within the composite. The Scherrer formula (D= 0.9 λ/βcosθ) is employed to estimate the average size of the nanocrystals, calculated from the three most substantial peaks corresponding to the (101), (002), and (110) indices [31]. The average crystallite size value for ZnS/CdS: Ag nanoparticles was approximately 18.88 nm. The XRD patterns do not exhibit any additional peaks, indicating no secondary phase in the ZnS/CdS: Ag nanocomposite.

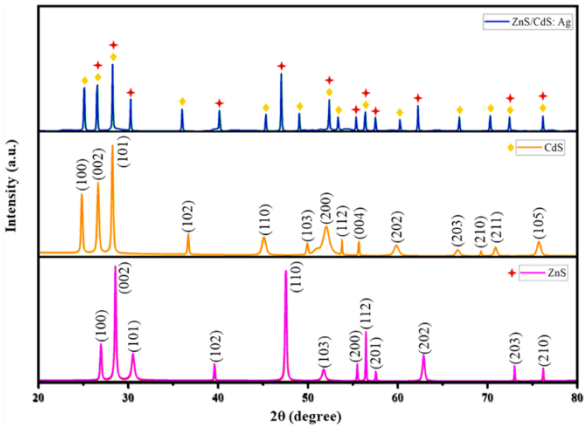

Fig. 2. The X-ray diffraction pattern of the synthesized samples

3.2. Functional Group Analysis

The results of the FTIR investigation are presented in Figure 3, which aimed to investigate the bonding environments in the samples. The FTIR analysis revealed the different vibration modes of nanopowders. The frequencies of all analysed vibrational bands are presented in Fig. 3. In the ZnS sample, the broad and strong band near 3450 cm^{-1} appears typically due to O–H stretching absorbed on the surface of water molecules. The existence of a band at around 2900 cm^{-1} suggests the symmetric and asymmetric (C-H) vibrations of the CH_2 groups in acetate. In addition, the C=O stretching mode is indicated by a peak at 1637 cm^{-1}, which is present in the carboxylic group (-COOH) of zinc acetate. The frequencies between 1140 cm^{-1} and 1070 cm^{-1} correspond to vibration modes related to the stretching of the C–N bond. The ZnS band, which corresponds to zinc sulfide nanoparticles, is identified by the peak at 624 cm^{-1}. Furthermore, the synthesized CdS nanoparticles exhibit functional group peaks at 3450, 1637, 1140, and 724 to 458 cm^{-1}, which correspond to the O–H, C=O, C–N, and Cd–S stretching vibrations, respectively [33-36]. The FTIR results confirmed the successful formation of the ZnS/CdS: Ag nanocomposite, revealing the presence of functional groups such as O–H, C=O, C–N, Zn–S, and Cd–S. When ZnS and CdS were combined, the bands at 3459 cm^{-1} (corresponding to O–H stretching) and 1140 cm^{-1} (corresponding

[DOI: 10.22068/ijmse.3784]

to C–N stretching) exhibited a decrease in intensity. This reduction in intensity points to a composition or interaction between the zinc sulfide nanopowders and the cadmium sulfide nanopowders. On the other hand, silver dopant in the nanocomposite affects the bonds and leads to a change in absorption intensity. So, changes in the intensity of certain vibrating bands can be seen between the samples (Fig. 3).

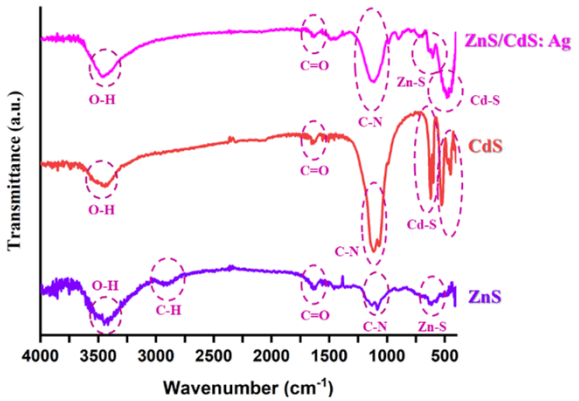

Fig. 3. FT-IR absorption spectra of the synthesized samples

The absorption intensity of the peaks at 3450, 1637, 1140, 624, and 458 cm^{-1} in the ZnS/CdS: Ag has changed relative to pure ZnS and CdS, and this decrease in the intensity of the peaks indicates the substitution of Ag^{+} ions in the composite network. As a result of the presence of impurities, the intensities of the bands changed with the addition of silver nanopowders, and no other absorption bands were observed in the composite sample [35].

3.3. Morphological Studies and Chemical Composition

Energy-dispersive X-ray spectroscopy (EDX) and field emission scanning electron microscopy (FESEM) were utilized to examine the morphology and chemical composition of the ZnS and CdS nanoparticles and the ZnS/CdS: Ag nanocomposite. As shown in Figure 4 (a, b, and c), the FESEM images reveal that the synthesized nanoparticles have distinct semi-spherical and rod-like shapes. The semi-spherical ZnS/CdS: Ag nanoparticles have an average size of 180 nm, while the rod-shaped particles feature a hexagonal top with an average diameter of 250 nm.

The chemical composition of the synthesized nanocomposite was further analyzed using energy-dispersive X-ray spectroscopy (EDX) and elemental mapping techniques. Figure 5 shows the EDX spectrum of the nanocomposites, highlighting the peaks corresponding to the elements Zn, Cd, S, O, and Ag. The elemental mapping color composition for the nanocomposites is presented in the exact figure, demonstrating the presence and uniform distribution of Zn, Cd, S, O, and Ag throughout the doped nanocomposite.

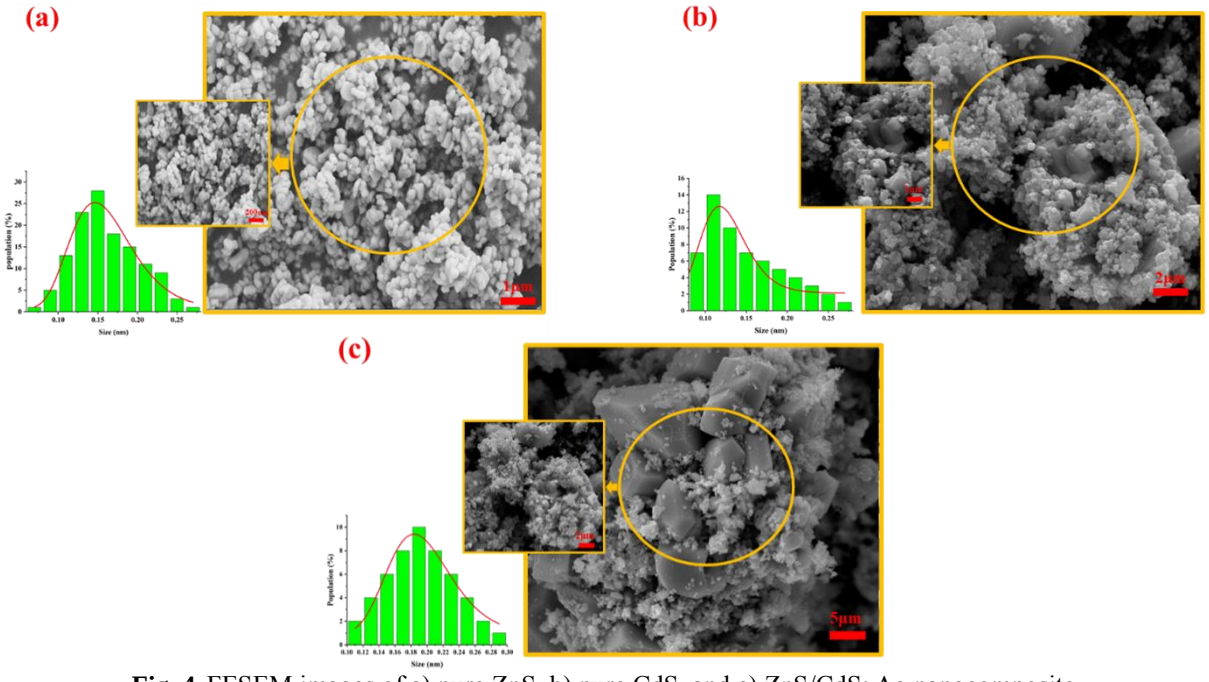

Fig. 4. FESEM images of a) pure ZnS, b) pure CdS, and c) ZnS/CdS: Ag nanocomposite

[DOI: 10.22068/ijmse.3784]

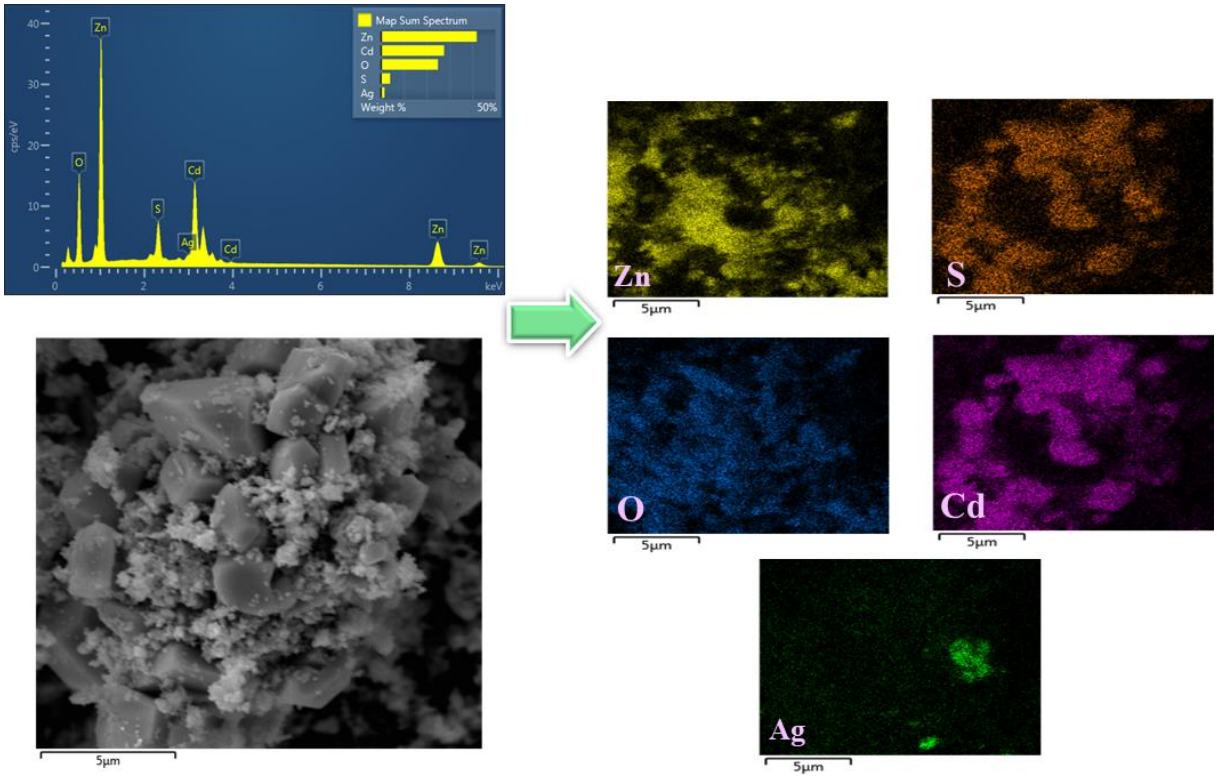

Fig. 5. EDAX and Map elemental of the ZnS/CdS: Ag nanocomposite

3.4. UV–Vis Analysis

UV-Vis absorption spectroscopy is a crucial technique for identifying nanoparticle absorption bands and bandgap energies, which are closely linked to their structural properties [31-34]. As nanoparticle size decreases, their surface area increases, potentially enhancing their adsorption efficiency and increasing bandgap energy. For this study, the UV-Vis spectra of the synthesized ZnS, CdS, and ZnS/CdS: Ag nanoparticles were obtained by dispersing them in deionized water and subjecting the solutions to an ultrasonic bath for 20 minutes to ensure thorough dispersion. Figure 6 (a, b, and c) compares the UV-Vis spectra of ZnS, CdS, and the ZnS/CdS: Ag nanocomposite, allowing for the determination of their absorption characteristics and bandgap energies. The absorption edges for ZnS, CdS, and ZnS/CdS: Ag was approximately 240 nm, 230 nm, and 225 nm, respectively, as illustrated in Figure 6 (a, b, and c).

The band gap energy of all samples can be examined through the UV–Vis spectra employing the Tauc relation [31],

$$\alpha h\nu = A(h\nu - E_g)^n \quad (1)$$

Where A is a proportionality constant, E_g is the energy in the bandgap, v is the photon frequency, α is the absorption coefficient, and n is the constant that determines the optic transmission. Two different kinds of transfer may be observed: direct and indirect. Indirect transfers were determined as $n = \frac{1}{2}$, while direct transfers were determined as n= 2. The tangent line shows the band energy on the Taucs plot. The direct bandgap values of ZnS, CdS, and ZnS/CdS: Ag nanocomposite were equal to 5.5, 5.3, and 5.2 eV, respectively. Similar large bandgap values also were reported in Cu and Ni doping ZnS nanoparticles [38].

3.5. IBIL Spectra

A crucial analytical technique is ion beam-induced luminescence (IBIL) characterization. The information it offers refers to the impurities, defects, and chemical compounds present in the material [36, 37]. During irradiation, the target materials emit photons [4, 5]. The responses of the produced samples to ionoluminescence were studied using focused proton beam irradiation (2.25 MeV), and the results are shown in Figure 7. The pure ZnS sample demonstrated a weak peak between 580-610 nm, whereas the pure CdS sample showed an intense peak at around 570 nm under the same irradiation situations.

[DOI: 10.22068/ijmse.3784]

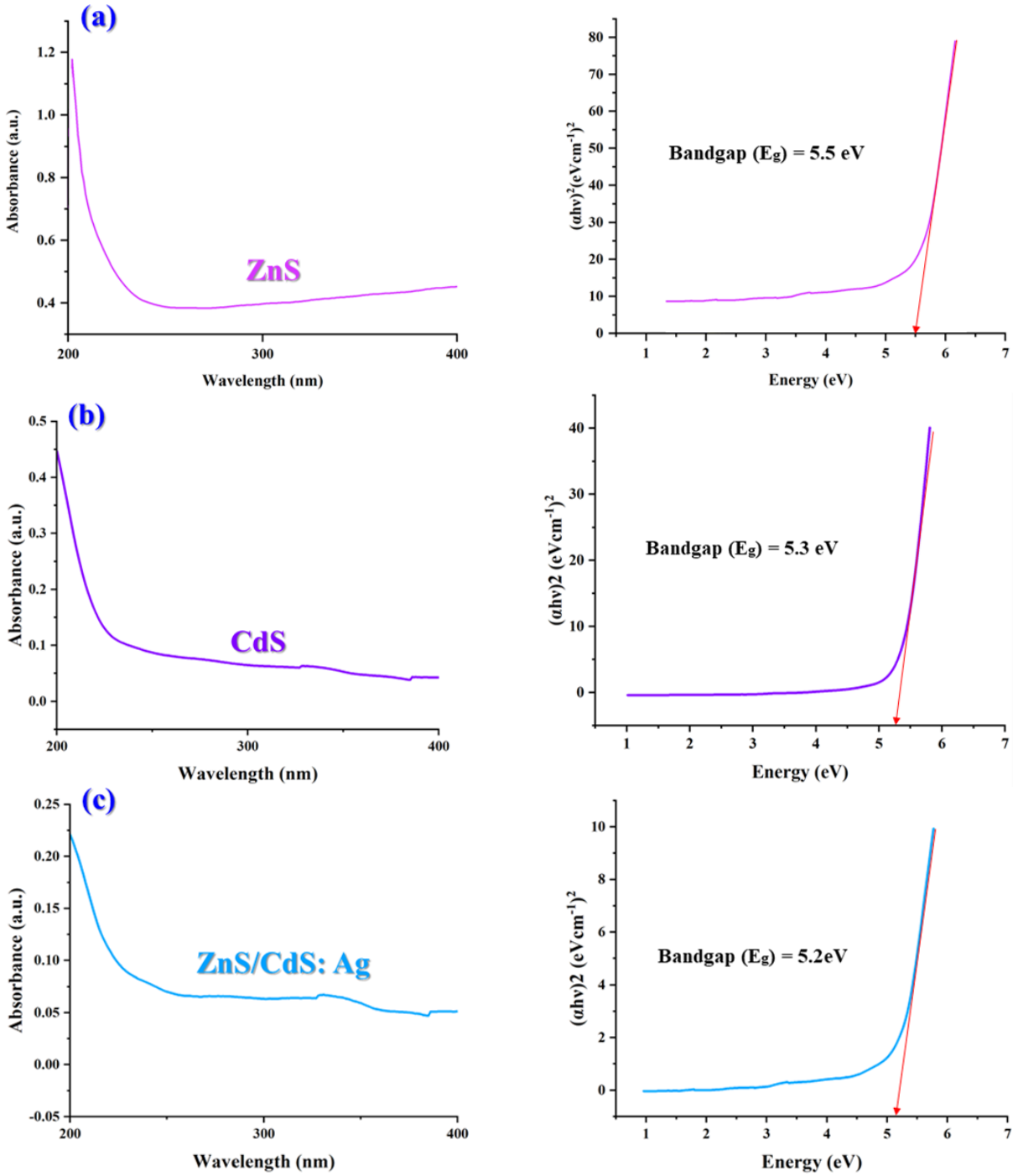

Fig. 6. UV–Vis absorption spectra and the $(\alpha h\nu)^2$ versus hν curves for the optical band gap determination of a) ZnS, b) CdS, and c) ZnS/CdS: Ag nanocomposite

The ZnS/CdS: Ag nanocomposite exhibited the most strong emission peak at around 560 nm. As a result, the Ag-doped ZnS/CdS: Ag nanocomposite exhibited the most potent and intense emission peak.

3.6. Scintillation Properties

Figure 8 presents the scintillation pulse height spectra for the PVA thin film as a baseline, along with the ZnS, CdS, and ZnS/CdS: Ag nanocomposites (composed of polymer and scintillation filler) under alpha irradiation. The count rate intensity for the Ag-doped ZnS/CdS nanocomposite films was significantly higher than that of the pure ZnS and CdS samples.

[DOI: 10.22068/ijmse.3784]

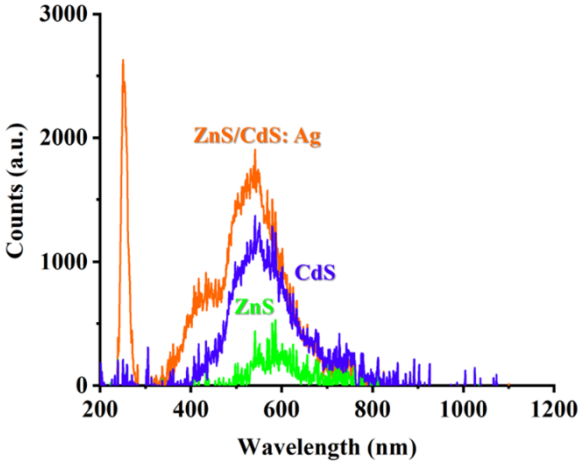

Fig. 7. IBIL spectrum of pure samples and Ag-doped ZnS/CdS nanocomposite

This indicates that the ZnS/CdS: Ag filler is crucial in the detection response and overall count rate. Incorporating ZnS and CdS nanoparticles into the hybrid film enhanced the position and intensity of the central peak in the count rate. The observed interaction between the nanoparticles and alpha particles appears to boost the production of scintillation light in the Ag-doped ZnS/CdS nanocomposite. This finding suggests that the nanocomposite can effectively convert invisible ionizing radiation into visible photons, making it a promising candidate for radiation sensing in future optical and medical applications. The measuring alpha radiation detection procedure was conducted according to the schematic setup shown in Figure 9.

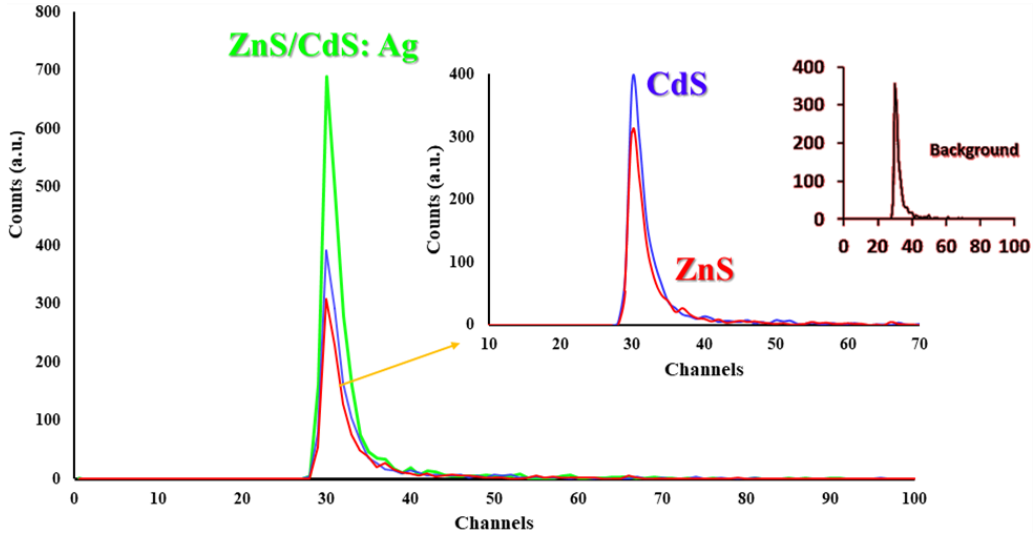

Fig. 8. Pulse height spectra of the pure ZnS, CdS, and Ag-doped ZnS/CdS nanocomposite

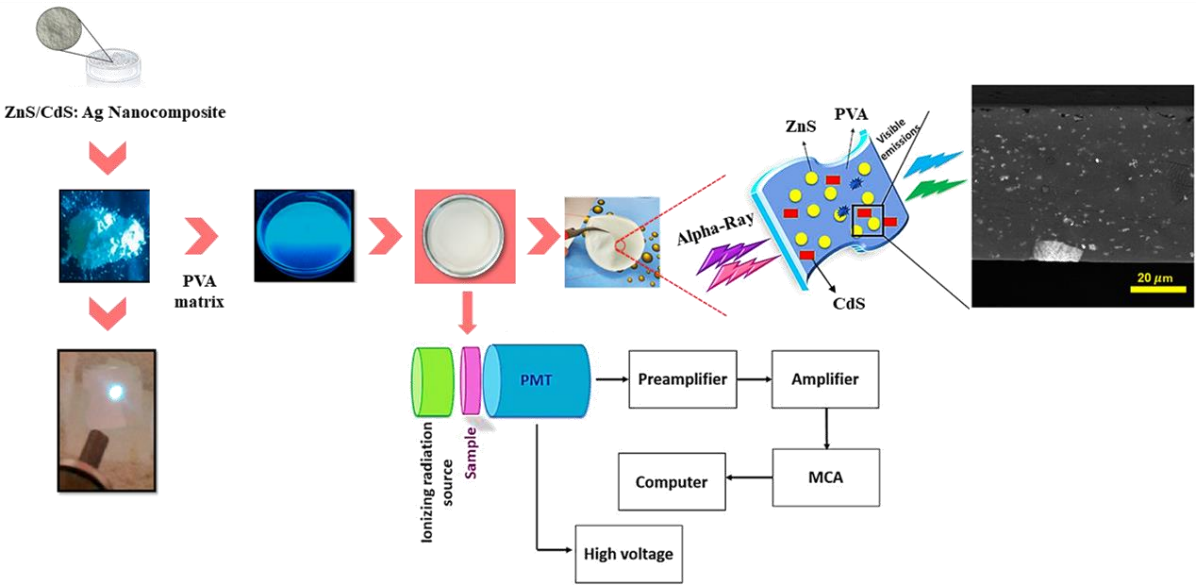

Fig. 9. Brief schematic of scintillation of the flexible scintillator films and experimental set-up

[DOI: 10.22068/ijmse.3784]

The net counting rate and absolute efficiency of the produced composite films were determined. The calculation of the absolute counting efficiency (ε) for the samples was performed using equation (2) [1, 9]:

$$\varepsilon = \frac{r_{net}}{A} \quad (2)$$

A is the alpha source activity, and r_{net} is the net counting rate. In our experiment, the activity of the ^{241}Am point source was reduced by half, taking into account the 2π geometry of the source. The absolute efficiency of ZnS, CdS, and ZnS/CdS: Ag were around 47%, 59%, and 88%, respectively.

4. CONCLUSIONS

In conclusion, this study introduces an innovative method for creating flexible thin films with a PVA matrix combined with sulfide semiconductors. It highlights the importance of customized band energy levels, affordable approaches, and promising applications in intelligent textiles and sensor technologies for the future. A highly luminous ZnS/CdS: Ag nanocomposite was synthesized using a simple chemical process. The combination of structured ZnS/CdS: Ag composite nanoparticles within a PVA matrix produced a flexible and soft thin film. The results of XRD confirmed the presence of characteristic peaks corresponding to ZnS and CdS within the synthesized nanocomposite structure. The synthesized ZnS/ CdS: Ag nanocomposite exhibited a range of shapes, such as cubic, rod-like, and semi-spherical, with an average diameter ranging from 180 to 250 nm. The ZnS/CdS: Ag nanocomposite demonstrated enhanced optical sensitivity relative to pure ZnS and CdS when exposed to ion beam and alpha irradiations and also showed acceptable scintillation properties at room temperature. The results indicate that the ZnS/ CdS: Ag nanocomposite film presents potential for various applications in optoelectronic devices.

ACKNOWLEDGMENTS

The authors thank the Iranian National Elites Foundation for funding this study. We also would like to sincerely thank Parto Negar Shahab Company -Radonik for their invaluable assistance and support in this research.

CREDIT AUTHORSHIP CONTRIBUTION STATEMENT

Maryam Hajiebrahimi: Writing–review & editing, Writing–original draft, Methodology, Synthesis, Data curation, Software, Resources. Sanaz Alamdari: Writing–review & editing, Investigation, Formal analysis, Data curation, Conceptualization. Omid Mirzaee: Writing–review & editing, Visualization, Validation, Supervision.

DECLARATION OF COMPETING INTEREST

The authors declare that they have no known competing financial interests or personal relationships that could have appeared to influence the work reported in this paper.

DATA AVAILABILITY

All data generated or analysed during this study are included in this published article.

REFERENCES

[1]. M. Hosseinpour, H. Abdoos, O. Mirzaee, and S. Alamdari, "Fabrication and characterization of a new flexible ionizing ray sensor based on lead tungstate ($PbWO_4$)," Ceram. Int., no. September, 2022, https://doi.org/10.1016/j.ceramint.2022.09.362.

[2]. Azadmehr, S., Jafat Taftreshi, M., Alamdari, S.: Synthesis, characterization and scintillation response of $ZnWO_4$-GO nanocomposite. J. Compos. Compd 4(12), 158–162 (2022).

[3]. X. Wang et al., "Color-tunable X-ray scintillation based on a series of isotypic lanthanide–organic frameworks †," Chem. Commun., 2020, 56, 233-236, https://doi.org/10.1039/C9CC08114C.

[4]. M. J. Tafreshi and S. Alamdari, "Facile synthesis of ZnO/CWO nanocomposite with brilliant enhanced optical response," Appl. Radiat. Isot., Volume 180, 2022, 110050, ISSN 0969-8043, https://doi.org/10.1016/j.apradiso.2021.110050.

[5]. Sanaz Alamdari, Mohammad Hosein Majles Ara, Majid Jafar Tafreshi, "Synthesize and optical response of ZnO/$CdWO_4$: Ce nanocomposite with high

[DOI: 10.22068/ijmse.3784]

sensitivity detection of ionizing radiations," Opt. Laser Technol., Volume 151, 2022, 107990, ISSN 0030-3992, https://doi.org/10.1016/j.optlastec.2022.107990Get rights and content.

[6]. Y. Yoon, P. L. Truong, D. Lee, and S. H. Ko, "Metal-Oxide Nanomaterials Synthesis and Applications in Flexible and Wearable Sensors," ACS Nanoscience Au 2022 2 (2), 64-92, https://doi.org/10.1021/acsnanoscienceau.1c00029.

[7]. S. Alamdari, M. Jafar Tafreshi, M. Sasani Ghamsari, Preparation and characterization of gallium doped zinc oxide/polystyrene nanocomposite scintillator for alpha particles detection. Appl. Phys. A (2019)125: 450.

[8]. S. Alamdari, M.S. Ghamsari, M.J. Tafreshi, Novel scintillation properties by entrapping ZnO: Ga nanocrystals in epoxy polymer, Progress in Nuclear Energy, 130, (2020), 103495.

[9]. N. Heydarian, M. Raeisi, and S. Alamdari, "Development of flexible scintillation sensors based on Ag and Gd doped $CdWO_4$ nanocomposites," Applied Radiation and Isotopes, Volume 189, 2022, 110457, ISSN 0969-8043, https://doi.org/10.1016/j.apradiso.2022.110457.

[10]. Alamdari, S., Jafar Tafreshi, M., Sasani Ghamsari, M., Majles Ara, M.H.: Preparation and characterization of ZnO and $CdWO_4$ nanopowders for radiation sensing. Prog. Phys. Appl. Mater. 1(1), 14–18 (2021).

[11]. H. Ziluei, R. Azimirad, M. Mojtahedzadeh Larijani, and F. Ziaie, "Preparation and optimization of $CdWO_4$-polymer nano-composite film as an alpha particle counter," Nucl. Instruments Methods Phys. Res. Sect. A Accel. Spectrometers, Detect. Assoc. Equip., vol. 852, pp. 85–90, 2017, https://doi.org/10.1016/j.nima.2017.01.015.

[12]. Sahani, R.M., Kumari, C., Pandya, A. et al. Efficient Alpha Radiation Detector using Low Temperature Hydrothermally Grown ZnO:Ga Nanorod Scintillator. Sci Rep 9, 11354 (2019). https://doi.org/10.1038/s41598-019-47732-1.

[13]. S. Alamdari, M. J. Tafreshi, and M. S. Ghamsari, "Highly stable Ga-doped ZnO/ polystyrene nanocomposite film with narrow-band cyan emission," vol. 40, no. 11, pp. 0–9, 2022, DOI: 10.1088/1674-4926/43/12/122301.

[14]. Alamdari, S., Sasani, G.M., Afarideh, H., Mohammadi, A., Geranmayeh, S., Tafreshi, M.J., Ehsani, M.H., Majles ara M.H.,: Preparation and characterization of GO-ZnO nanocomposite for UV detection application. Opt. Mater. 92, 243–250 (2019b).

[15]. Mitra Madani, Mohammad Mansourian, Sanaz Almadari, Omid Mirzaee, Majid Jafar Tafreshi, Enhanced photosensitivity of heterostructure SiO_2/Bi_2WO_6/GO composite nanoparticles, Physica B: Condensed Matter, Volume 645, 2022, 414241, ISSN 0921-4526, https://doi.org/10.1016/j.physb.2022.414241.

[16]. Michael Shur, Wide band gap semiconductor technology: State-of-the-art, Solid-State Electronics, Volume 155, 2019, Pages 65-75, ISSN 0038-1101, https://doi.org/10.1016/j.sse.2019.03.020.

[17]. Chen X, Lou Y, Dayal S, Qiu X, Krolicki R, Burda C, Zhao C, Becker J. Doped semiconductor nanomaterials. J Nanosci Nanotechnol. 2005 Sep;5(9):1408-20. DOI: 10.1166/jnn.2005.310.

[18]. S. Alamdari, M. S. Ghamsari, and M. J. Tafreshi, "Progress in Nuclear Energy Novel scintillation properties by entrapping ZnO : Ga nanocrystals in epoxy polymer," Prog. Nucl. Energy, Volume 130, 2020, 103495, ISSN 0149-1970, https://doi.org/10.1016/j.pnucene.2020.103495.

[19]. Xu, LJ., Lin, X., He, Q. et al. Highly efficient eco-friendly X-ray scintillators based on an organic manganese halide. Nat Commun 11, 4329 (2020). https://doi.org/10.1038/s41467-020-18119-y.

[20]. Romain Génois, Stéphane Jobic, Guy Ouvrard, Florian Massuyeau, Romain Gautier, The crucial impact of cerium reduction on photoluminescence, Applied Materials Today, Volume 20, 2020, 100643, ISSN 2352-9407, https://doi.org/10.1016/j.apmt.2020.100643.

[DOI: 10.22068/ijmse.3784]

[21]. H. Ziluei, R. Azimirad, M. Mojtahedzade Larijani, F. Ziaie, Preparation and optimization of $CdWO_4$-polymer nano-composite film as an alpha particle counter, Nuclear Inst. and Methods in Physics Research, A 852 (21) (2017) 85–90, https://doi.org/10.1016/j.nima.2017.01.015.

[22]. Krishnan, R., Ayyanar, M., Kasinathan, A. and Kumar, P., 2018. Birefringence, photo luminous, optical limiting and third order nonlinear optical properties of glycinium phosphite (glp) single crystal: A potential semi organic crystal for laser and photonics applications. Materials Research, 21(2), p.e20170329.N. https://doi.org/10.1590/1980-5373-MR-2017-0329

[23]. S. Alamdari, M.S. Ghamsari, M.J. Tafreshi, Optimization of Gallium concentration to improve the performance of ZnO nanopowders for nanophotonic applications, Ceramics International, 46 4 (2020)4484-4492.

[24]. Alamdari, S., Haji Ebrahimi, M., Mirzaee, O., Jafar Tafreshi, M., Majlesara, M.H., Tajali, M., Sasani Ghamsari, M. and Mohammadi, A., 2022. Cerium doped Tungsten-Based Compounds for Thermoluminescence Application. Progress in Physics of Applied Materials, 2(1), pp.35-40., DOI: 10.22075/PPAM.2022.27086.1028.

[25]. Anandan, K., Rajesh, K. & Rajendran, V. Size, morphology and optical properties of zirconia (ZrO_2) nanostructures synthesized via the facile ionic surfactant-assisted solvothermal method. J Mater Sci: Mater Electron 28, 13420–13425 (2017). https://doi.org/10.1007/s10854-017-7180-3.

[26]. Hemmati, Mohammad, Majid Jafar Tafreshi, Mohammad Hossein Ehsani, and Sanaz Alamdari. "Highly sensitive and wide-range flexible sensor based on hybrid $BaWO_4$@ CS nanocomposite." Ceramics International 48, no. 18 (2022): 26508-26518. https://doi.org/10.1016/j.ceramint.2022.05.347.

[27]. S. Alamdari, M. Jafar Tafreshi, M. Sasani Ghamsari, Preparation and characterization of gallium doped zinc oxide/polystyrene nanocomposite scintillator for alpha particles detection. Appl. Phys. A (2019)125: 450.

[28]. Hosseinpour, M., Mirzaee, O., Alamdari, S., Menéndez, J.L., Abdoos, H.: Development of a novel flexible thin PWO(Er)/ZnO(Ag) nanocomposite for ionizing radiation sensing. J. Alloy. Compd. 967, 171678 (2023b).

[29]. Maryam Hajiebrahimi, Sanaz Alamdari, Omid Mirzaee, and Mohammad Tajally. "Luminescence Investigation of Ce Doped ZnO/$CdWO_4$ Nanocomposite." Advanced Ceramics Progress 8, no. 3 (2022): 8-12, https://doi.org/10.30501/acp.2022.363264.1102.

[30]. Kundu, J., Satpathy, B.K. and Pradhan, D., 2019. Composition-controlled CdS/ZnS heterostructure nanocomposites for efficient visible light photocatalytic hydrogen generation. Industrial & Engineering Chemistry Research, 58(51), pp.22709-22717, https://doi.org/10.1021/acs.iecr.9b03764.

[31]. Farahani, M.M.H., Hajiebrahimi, M., Alamdari, S., Najafzadehkhoee, A., Khounsaraki, G.M., Agheb, M., Kostiuk, V., Puškárová, A., Bučková, M., Pangallo, D. and Hvizdoš, P., 2024. Synthesis and antibacterial activity of silver doped zinc sulfide/chitosan bionanocomposites: A new frontier in biomedical applications. International Journal of Biological Macromolecules, 280, p.135934, https://doi.org/10.1016/j.ijbiomac.2024.135934.

[32]. Lalithadevi, B., Rao, K.M. and Ramananda, D., 2018. Investigations on structural and optical properties of starch capped ZnS nanoparticles synthesized by microwave irradiation method. Chemical Physics Letters, 700, pp.74-79, https://doi.org/10.1016/j.cplett.2018.04.010.

[33]. Kannan, S., Subiramaniyam, N.P. & Sathishkumar, M. A novel green synthesis approach for improved photocatalytic activity and antibacterial properties of zinc sulfide nanoparticles using plant extract of Acalypha indica and Tridax procumbens. J Mater Sci: Mater Electron 31, 9846–9859

[DOI: 10.22068/ijmse.3784]

(2020). https://doi.org/10.1007/s10854-020-03529-x.

[34]. lsi, S. and Pushpanathan, K., 2021. Room temperature ferromagnetism in ZnS and ZnO nanoparticles. Inorganic and Nano-Metal Chemistry, 51(4), pp.590-600, https://doi.org/10.1080/24701556.2020.1799405.

[35]. Shahriari, E., Farsani, Z.M., Varnamkhasti, M.G. et al. Linear and non-linear optical properties of Ag doped ZnS thin film. Opt Quant Electron 49, 151 (2017). https://doi.org/10.1007/s11082-017-0991-x.

[36]. Mohammad Banari, Nafiseh Memarian, Pankaj Kumar, Shujie You, Alberto Vomiero, Isabella Concina,CeO_2:ZnO hybrid nanorods for self-powered UV-photodetectors, Ceramics International, 2024. https://doi.org/10.1016/j.ceramint.2024.10.254.

[37]. Al-Shemri, M.I., Aliannezhadi, M., Ghaleb, R.A. et al. Au-$H_2Ti_3O_7$ nanotubes for non-invasive anticancer treatment by simultaneous photothermal and photodynamic therapy. Sci Rep 14, 25998 (2024). https://doi.org/10.1038/s41598-024-75862-8.

[38]. Khalid T. Al- Rasoul, Nada K. Abbas, Zainb J. Shanan,Structural and Optical Characterization of Cu and Ni Doped ZnS Nanoparticles, International Journal of Electrochemical Science,Volume 8, Issue 4, 2013, Pages 5594-5604. https://doi.org/10.1016/S1452-3981(23)14706-7.

[DOI: 10.22068/ijmse.3784]